Available online at : http://josi.ft.unand.ac.id/

Jurnal Optimasi Sistem Industri

| ISSN (Print) 2088-4842 | ISSN (Online) 2442-8795 |

Research Article

Optimal PLA+ 3D Printing Parameters through Charpy Impact Testing: A Response Surface Methodology

Engelbert Harsandi Erik Suryadarma [a, b], Pringgo Widyo Laksono [a,*], Ilham Priadythama [a]

[a] Department of Industrial Engineering, Universitas Sebelas Maret, Surakarta, Indonesia
[b] Department of Industrial Engineering, Universitas Atma Jaya Yogyakarta, Yogyakarta, Indonesia

[*] Corresponding Author: pringgo@ft.uns.ac.id

DOI: 10.25077/josi.v23.n1.p76-91.2024 **Submitted** : March 16, 2024; **Accepted** : June 3, 2024; **Published** : July 10, 2024

ABSTRACT

Additive manufacturing (AM) has revolutionized the manufacturing sector, particularly with the advent of 3D printing technology, which allows for the creation of customized, cost-effective, and waste-free products. However, concerns about the strength and reliability of 3D-printed products persist. This study focuses on the impact of three crucial variables—infill density, printing speed, and infill pattern—on the strength of PLA+ 3D-printed products. Our goal is to optimize these parameters to enhance product strength without compromising efficiency. We employed Charpy impact testing and Response Surface Methodology (RSM) to analyze the effects of these variables in combination. Charpy impact testing provides a measure of material toughness, while RSM allows for the optimization of multiple interacting factors. Our experimental design included varying the infill density from low to high values, adjusting printing speeds from 70mm/s to 100mm/s, and using different infill patterns such as cubic and others. Our results show that increasing infill density significantly boosts product strength but also requires more material and longer processing times. Notably, we found that when the infill density exceeds 50%, the printing speed can be increased to 100mm/s without a notable reduction in strength, offering a balance between durability and production efficiency. Additionally, specific infill patterns like cubic provided better strength outcomes compared to others. These findings provide valuable insights for developing stronger and more efficient 3D-printed products using PLA+ materials. By optimizing these parameters, manufacturers can produce high-strength items more efficiently, thereby advancing the capabilities and applications of 3D printing technology in various industries.

Keywords: additive manufacturing, PLA+ 3D printing parameters, Charpy impact testing, response surface methodology

INTRODUCTION

Additive manufacturing, commonly known as 3D printing, has fundamentally transformed traditional manufacturing processes [1]–[3]. This innovative technology enables the layer-by-layer creation of three-dimensional objects based on digital models, diverging significantly from traditional subtractive methods [4], [5]. Its adaptability and versatility have driven its widespread adoption across various industries, including aerospace, healthcare, and automotive sectors [6]–[8]. Beyond rapid prototyping, 3D printing now facilitates the direct production of end-use components [9], reshaping supply chains with its on-demand manufacturing capability [10]. Continued technological advancements are enhancing the integration of digital design with additive manufacturing, opening new avenues for customization, efficiency, and sustainability [11], [12]. This evolution positions 3D printing at the forefront of modern manufacturing methodologies, driving innovation across industries.

Additive manufacturing stands out for its significant reduction in material waste compared to traditional methods [13], [14]. Unlike subtractive processes that often lead to substantial wastage through cutting and shaping [15], AM builds objects layer by layer, using only the necessary material. This approach not only minimizes waste but also positions AM as a sustainable choice in manufacturing, aligning with increasing environmental concerns among industries and consumers. Beyond sustainability, AM offers unprecedented design flexibility, enabling the

production of intricate and customized products that were previously impractical [16], [17]. This capability has transformative implications across sectors: from personalized medical implants tailored to individual patient needs to aerospace components optimized for performance and weight. Moreover, the ability to rapidly prototype and iterate designs accelerates the product development cycle, empowering companies to innovate and bring new solutions to market swiftly and efficiently.

Fused Deposition Modeling (FDM) is a widely used additive manufacturing technique in 3D printing known for its efficiency and versatility [18], [19]. This method involves heating a thermoplastic filament, typically ABS or PLA, to its melting point and extruding it through a nozzle onto a build platform in precise layers to form the desired object [20], [21]. FDM offers several advantages, including cost-effectiveness, high precision, and the ability to create complex geometries with ease [22]. However, challenges such as limited material choices and the need for post-processing highlight the necessity for ongoing research and development to expand its capabilities across academic and industrial applications.

Fused Deposition Modeling (FDM) in 3D printing relies on various critical parameters to achieve precise and dependable fabrication [21]–[23]. These parameters encompass layer height, nozzle diameter, printing speed, extruder temperature, bed temperature, infill pattern, infill density, and material type. Layer height directly influences the thickness of each deposited layer, impacting the resolution and surface finish of the printed object [24]. Meanwhile, nozzle diameter affects extrusion precision, and printing speed determines both the duration of printing and the quality of the final part. Defined as the rate at which the printer's extruder deposits material, printing speed plays a pivotal role in optimizing printing efficiency and ensuring part strength. Finding the optimal printing speed is crucial to achieve proper bonding between successive layers and to mitigate issues like extrusion inconsistencies and warping [23], [25]. High printing speeds can compromise layer adhesion, leading to weakened interlayer bonds and reduced structural integrity. Conversely, excessively slow speeds may prolong printing time and exacerbate problems related to thermal degradation of filament materials. Therefore, striking a balance between printing speed and part quality is essential for producing robust and mechanically sound printed objects. This approach ensures efficient printing while maintaining the integrity and durability required for various applications in additive manufacturing.

The choice of infill pattern significantly impacts both the internal structure and mechanical properties of printed parts. Common infill patterns such as rectilinear, grid, triangular, honeycomb, cubic, gyroid, and concentric each offer distinct advantages in terms of strength, weight efficiency, and material usage [23]. For example, honeycomb patterns are known for their high strength-to-weight ratio, making them ideal for applications requiring robustness with minimal material consumption. On the other hand, rectilinear patterns offer simplicity and ease of printing while providing adequate support and structural reinforcement [26]. Infill density, which refers to the proportion of interior space filled with infill material, deeply influences the mechanical strength and load-bearing capacity of printed objects. Higher infill densities result in denser internal structures, thereby enhancing overall strength and rigidity. However, increasing infill density also leads to greater material usage and longer printing times. Balancing infill density with specific structural requirements is crucial for optimizing part performance while minimizing material waste and production costs [27].

PLA+ (Polylactic Acid) has gained popularity in 3D printing due to its biodegradability and ease of use [28], [29]. Despite its widespread utilization, there is a notable lack of comprehensive research on the optimal printing parameters needed to achieve the highest strength in PLA+ prints. Existing studies have examined various mechanical properties of PLA+ such as tensile strength and hardness, but they often fail to identify the ideal printing conditions, including temperature, layer thickness, and infill patterns, which are crucial for enhancing mechanical performance. Addressing this research gap is essential for maximizing the mechanical properties of PLA+ and unlocking its full potential in applications ranging from prototyping to functional end-use parts. A thorough investigation into these printing parameters could lead to significant advancements in the performance and durability of PLA+ 3D prints.

The use of PLA+ in 3D printing is expanding across various industries, including medical, automotive, and aerospace sectors. In the medical field, PLA+ is utilized for creating biodegradable implants, surgical guides, and custom

 DOI: 10.25077/josi.v23.n1.p76-91.2024

anatomical models for pre-surgical planning [30]-[32]. In the automotive industry, PLA+ is employed to produce prototypes and small components, such as dashboard elements and custom fixtures, due to its ease of printing and cost-effectiveness [33]-[36]. In the aerospace sector, PLA+ is used for creating lightweight, non-critical components like jigs and fixtures for assembly processes, as well as for prototyping complex parts to streamline design and testing phases [37], [38]. These examples demonstrate how PLA+ 3D printing is contributing to advancements and efficiencies in a range of high-tech industries.

However, despite these advancements, there is a noticeable gap in the research concerning the interplay of infill density, infill pattern, and printing speed in 3D printing. Many researchers do not adequately clarify how these parameters interrelate, with most current studies isolating each parameter and seeking to optimize them individually. This study seeks to address this gap by integrating these three vital parameters using response surface methodology with a full factorial design, offering a novel and more robust solution. This approach allows for a comprehensive examination of the interactions between parameters, enabling the identification of optimal combinations for producing high-strength products. By simultaneously determining the best settings for these parameters, the study aims to provide a deeper and more holistic understanding essential for advancing additive manufacturing technologies.

Table 1 provides an overview of research on the mechanical properties of PLA+ material in the context of 3D printing. While several studies have examined key parameters such as infill density, infill pattern, printing speed, nozzle size, and extruder temperature, there is considerable variation in the testing procedures employed. For instance, only a few articles have utilized the impact test procedure, while others predominantly focus on tensile testing. Furthermore, existing studies often use small sample sizes, limiting the generalizability of their findings. To address these limitations, this study will employ response surface methodology with a full factorial design, allowing for a more comprehensive exploration of the relationship between printing parameters and mechanical properties. By fabricating 320 specimens, this approach aims to provide robust experimental data to elucidate optimal parameter settings while considering design requirements and cost-effectiveness.

Table 1. Overview of Studies on the Mechanical Characteristics of 3D-Printed Components Using PLA+ Material.

No.	Author	Research	Mechanical test	Sample size
1	Yadav et al. [39]	infill density, lay bed position	Tensile	not diclared
2	Yilan et al. [40]	Infill density, Infill pattern, printing speed, used anova	Tensile	@1 total 18
3	Tura et al. [41]	infill density, print speed, shell count	Tensile	not diclared
4	Bhandarkar et al. [42]	Infill pattern, infill density, extruder temperature, taguchi	Tensile, roughness	@1
5	Mani et al. [43]	layer thickness, infill density, extruder temperature, taguchi	Tensile, roughness	@1
6	Mishra et al. [44]	carbon fiber PLA, Infill pattern, infill density, printing speed, used anova	Tensile dan flexural	54 speciment
7	Travieso-Rodriguez et al. [45]	ABS, PLA, PLA Wood,	Tensile dan flexural	27 speciment
8	Khawly et al. [46]	infill density	Impact testing	@1
9	Pandzic et al. [47]	infill density, compare ultimaker 3d print model	Tensile	@1
10	Hasan et al. [48]	storage 6 month and heat treatment at 57.5C	Tensile	96 speciment
11	Triyono et al. [49]	nozzle hole diameter 0.3; 0.4; 0.5; 0.6	Porosity and tensile	@1 total 4
12	Farayibi and Omiyale [50]	infill density, extruder temperature, Taguchi	Tensile, Impact, hardness	@1
13	The proposed research	Infill density, printing speed infill pattern use Response Surface Methodology	Impact	320 speciment

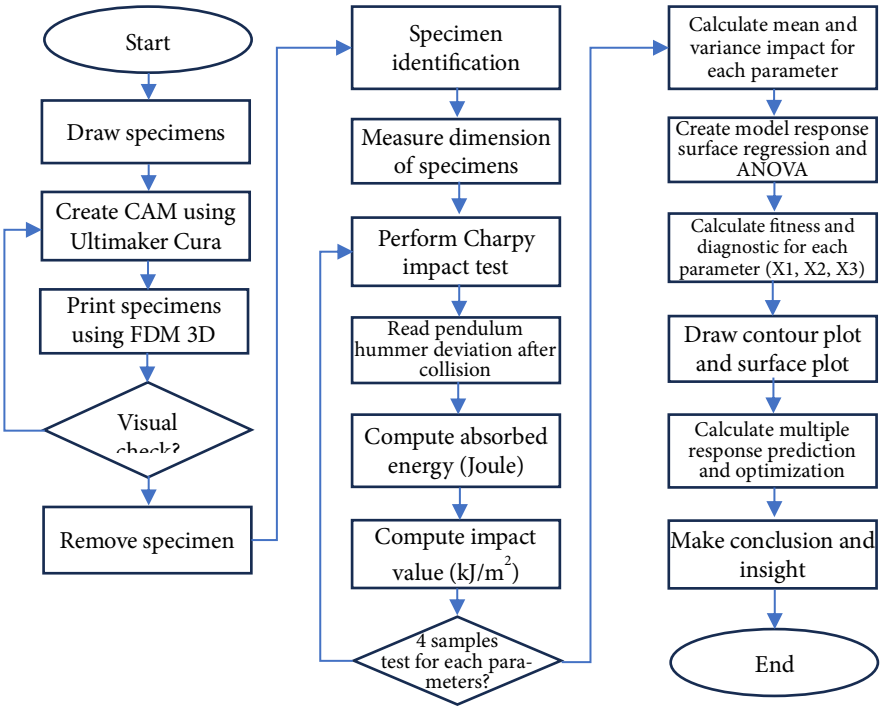

Figure 1. The design of the specimens by SolidWorks software and then Ultimaker Cura software for slicing and generating G-Code.

Utilizing response surface methodology not only enables the identification of optimal parameters by maximizing impact values but also allows the observation of each parameter's sensitivity to its impact value. This facilitates finding parameter settings that suit design requirements, eliminating the necessity of using only the parameters with the highest impact values. Instead, it enables the determination of other parameters with impact values close to the best, while maintaining an economical process and lightweight material. Moreover, understanding these interactions is essential for achieving high-strength products through additive manufacturing. By simultaneously identifying the best settings for infill parameters and printing speed, this research aims to provide comprehensive insights into optimizing additive manufacturing processes. These insights will be crucial for enhanced product development, ensuring that the produced parts are both robust and cost-effective.

METHODS

This article employs Response Surface Methodology (RSM) to determine the optimal parameters for the 3D printing process [44]–[46]. The identified parameters will serve as independent variables, while the impact values will be treated as dependent variables. The specific parameters selected, namely printing speed, infill density, and infill pattern, are based on the literature review in the previous section due to their significant impact on the strength of 3D printed results [39]–[41]. The experimental procedure is illustrated in Figure 1.

The first step of the experiment involves making the specimens. The design of the specimens was accomplished using SolidWorks software, with the files saved as .stl files. Following this, Ultimaker Cura software was used for slicing and generating G-Code, which was then executed on a 3D printing machine employing Fused Deposition Modeling (FDM) technology (see Figure 2). The fabrication of specimens and the subsequent Charpy Impact Tests adhere to the ASTM D6110 standards. ASTM D6110 is a standard test method established by ASTM International for determining the impact resistance of plastic specimens. Specifically, it describes the procedure for conducting the Izod pendulum impact resistance test, which measures the energy absorbed by a material during fracture. This test is crucial for evaluating the toughness and durability of plastic materials under sudden impacts.

A visual inspection is conducted to ensure that the specimens from the 3D printer are free from defects such as shrinkage and deformation. Any non-conforming specimens will be discarded. For each set of parameters, five

 DOI: 10.25077/josi.v23.n1.p76-91.2024

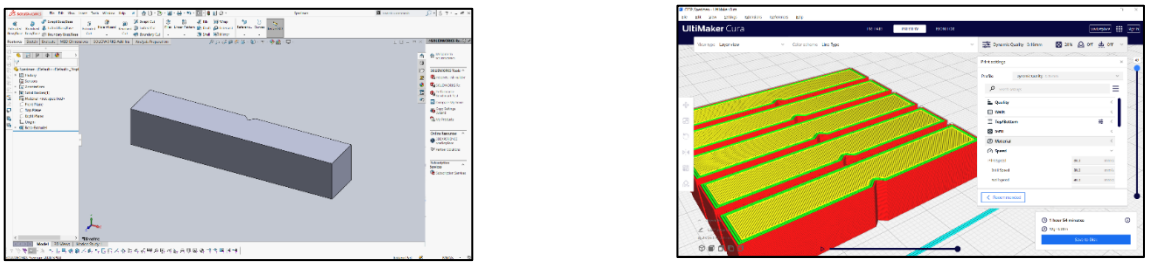

Figure 2. The design of the specimens by SolidWorks software and then Ultimaker Cura software for slicing and generating G-Code.

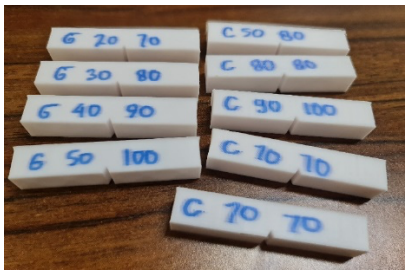

Figure 3. The specimens are ready for Charpy impact testing

specimens will be produced (four for testing and one as a backup). Once completed, the specimens will be labeled, measured, and prepared for Charpy impact testing, as shown in Figure 3. Charpy impact testing, a widely used technique for assessing material toughness, involves striking a notched specimen with a pendulum to measure the energy absorbed during fracture. This method is crucial for determining the suitability of materials for structural components, providing insights into their performance under dynamic loading conditions, and ensuring enhanced safety and reliability in real-world applications. In this study, Charpy impact testing is conducted on specimens created with varying parameters: infill density (ranging from 10% to 100% in increments), printing speed (70mm/s, 80mm/s, 90mm/s, and 100mm/s), and infill pattern (cubic and grid), as illustrated in Figure 4. The infill density increments were chosen based on the hypothesis that infill density significantly impacts the strength of the 3D printed part. The default printing speed in CURA software is 80mm/s, and the study aims to examine the effects of

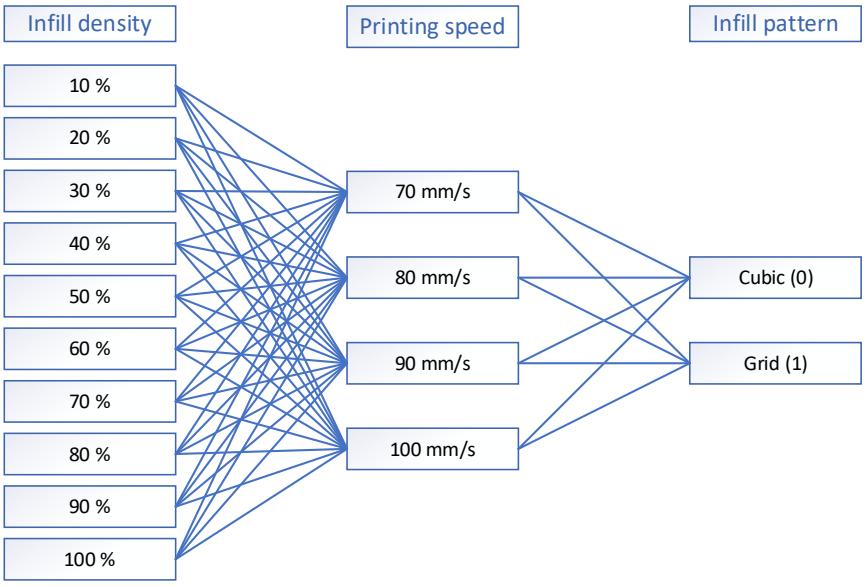

Figure 4. Production specimen using 3 parameter combination

Table 2. Analog Charpy impact machine specification

Specification	Unit
Hummer pendulum weight	6 kg
Hummer pendulum arm length (L)	500 cm
Hummer pendulum initial angle (α)	135 degrees
Specimen type	Metal, plastics, wood

increasing the speed up to 100mm/s. The choice of infill patterns is informed by a literature review and the default settings in CURA, which uses cubic infill for densities below 30% and grid infill for densities above 30%. The machine specifications are detailed in Table 2.

The testing mechanism is illustrated in Figure 5. In this figure, point A represents the axis of the impact machine, and L denotes the length of the hammer pendulum arm. The initial angle of the hammer pendulum is marked as α, while β indicates the angle position of the pendulum at its maximum deviation after the collision. Point B shows the initial position of the hammer pendulum, point C represents the position where the hammer collides with the specimen, and point D depicts the final position of the hammer pendulum at its maximum deviation after the impact. According to James Prescott Joule's law of conservation of energy, in the system depicted in Figure 5, the mechanical energy at points B, C, and D remains the same if external forces like air resistance are neglected, as shown in Equation (1). Mechanical energy comprises both potential and kinetic energy, as indicated in Equation (2). At points B and D, the pendulum is stationary, so only potential energy is present (kinetic energy = 0). However, at point C, where the height h = 0, only kinetic energy is present (potential energy = 0), as illustrated in Equation (3).

$$Em_B = Em_C = Em_D \tag{1}$$

$$Ep_B + Ek_B = Ep_C + Ek_C = Ep_D + Ek_D \tag{2}$$

$$Ep_B = Ek_C = Ep_D \tag{3}$$

where

$Em_B;\ Em_C;\ Em_D$ = Mechanic energy at position B; C; D(Joule)
$Ep_B;\ Ep_C;\ Ep_D$ = Potential energy at position B; C; D (Joule)
$Ek_B;\ Ek_C;\ Ek_D$ = Kinetic energy at position B; C; D (Joule)

The condition described in Equation 3 changes due to the collision between the pendulum hammer and the specimen at point C. Consequently, a portion of the energy is absorbed by the specimen, which is used to calculate the impact strength of the material. The absorbed energy is the difference between the potential energy before the collision (Ep_B) and the potential energy after the collision (Ep_D), as shown in Equation (4). The potential energy before the collision

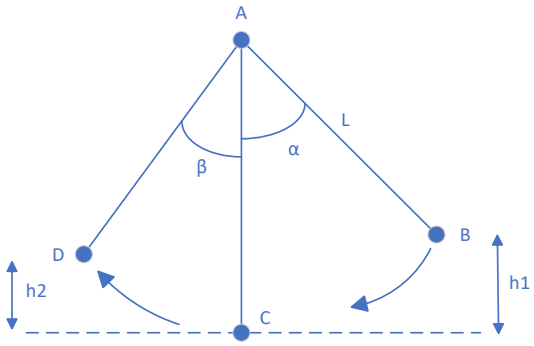

Figure 5. Free body diagram of Charpy impact machine

 DOI: 10.25077/josi.v23.n1.p76-91.2024

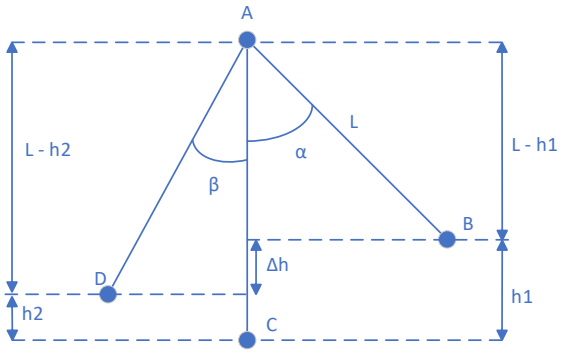

Figure 6. Free body diagram for absorbed energy calculation

(Ep_B) and after the collision (Ep_D) can be determined by knowing the heights h1 and h2, as illustrated in Figure 6 and Equation (5). Potential energy is calculated by multiplying the pendulum hammer mass, the gravitational constant, and the height of the hammer. Heights h1 and h2 can be determined using trigonometric equations for angles α and β, as shown in Equation (9).

$$E_{ABS} = Ep_B - Ep_D \tag{4}$$

$$E_{ABS} = mgh_1 - mgh_2 \tag{5}$$

$$E_{ABS} = mg(h_1 - h_2) \tag{6}$$

$$E_{ABS} = mg\Delta h \tag{7}$$

$$E_{ABS} = mg((L - h_2) - (L - h_1)) \tag{8}$$

$$E_{ABS} = mgL(cos\beta - cos\alpha) \tag{9}$$

where

E_{ABS} = Absorbed energy (Joule)
Ep_B = Potential energy at the position before the collision (Joule)
Ep_D = Potential energy at the maximum deviation position after the collision (Joule)
m = Pendulum hummer mass (kgs), the value is set 6 kgs
L = Pendulum hummer length (meter), the value is set 0.5m
α = Pendulum hummer starting position (degree), the value is set 1350)
β = Pendulum hummer at the maximum deviation position after the collision (degree)
G = Gravity constant (9.8 m/s^2)

The impact value is calculated by dividing the absorbed energy by the cross-sectional area of the collision, as shown in Equation (10). The measurement of the cross-sectional area is illustrated in Figure 7. The value is then multiplied by 1000 to convert the units from J/mm^2 to kJ/m^2.

$$I_{ch} = \frac{1000 .E_{ABS}}{A.W} \tag{10}$$

where

I_{ch} = Impact value (kJ/m^2)
A = see Figure 7 (mm)
W = Width of specimen, see Figure 8 (mm)

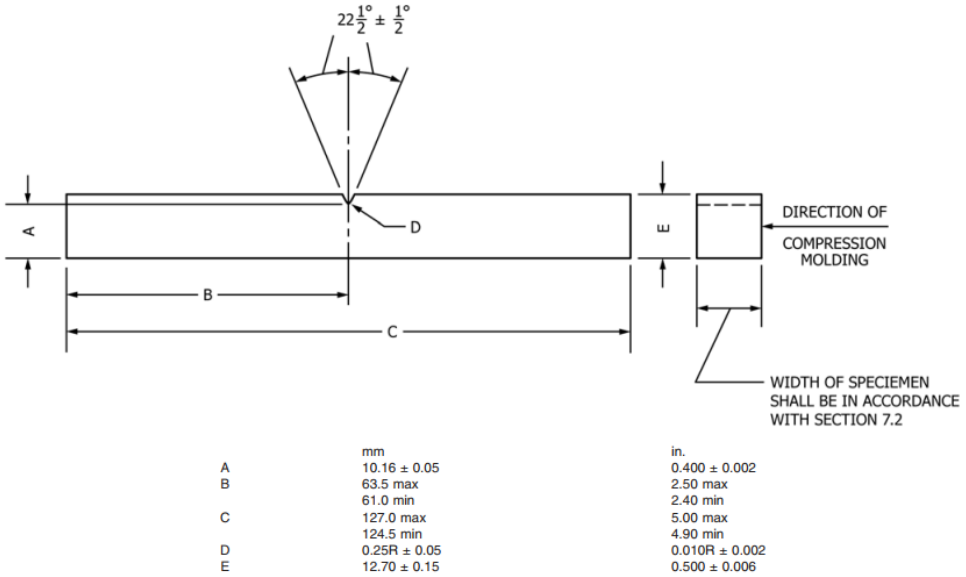

Figure 7. Dimensions of Charpy impact test specimen (ASTM D6110)

RESULT AND DISCUSSION

In this section, we present the results of sample testing, statistical calculations, and discussions to identify the optimum parameters among the three tested: infill density (X1), printing speed (X2), and infill pattern (X3) (0 = cubic, 1 = grid). For each parameter set, the impact values for the four samples are labelled A, B, C, and D, with the average impact value represented as μ (Y) and its variance as σ. This information is detailed in Table 3. Analysis of Variance (ANOVA) is employed to compare the means across multiple groups, a method widely used in experimental research. Table 4 displays the P-values for X1, X2, X3, X 1*X1 and X1*X3, which are all below the chosen significance level of 0.05. The sufficiently large F-values further support this analysis.

Table 3. Result of sample testing

Sample No.	X1 (%)	X2 (mm/s)	X3 (0, 1)	Impact Value (kJ/m²)					
				A	B	C	D	Y = μ	σ
1	100	70	0	165.325	173.660	193.326	185.194	179.376	152.852
2	90	70	0	177.015	173.489	172.740	161.470	171.178	45.366
3	80	70	0	102.610	83.336	129.307	106.059	105.328	355.523
4	70	70	0	90.815	68.577	68.699	57.720	71.453	193.118
5	60	70	0	94.520	57.834	72.189	83.205	76.937	245.301
6	50	70	0	40.525	64.823	75.629	33.684	53.665	392.947
7	40	70	0	68.496	37.188	75.629	57.584	59.724	280.793
8	30	70	0	57.777	64.772	43.756	43.851	52.539	109.905
9	20	70	0	36.925	68.644	37.042	33.856	44.117	269.552
10	10	70	0	14.693	27.199	27.242	57.686	31.705	334.879
11	100	70	1	153.410	157.020	168.641	161.184	160.064	42.787
12	90	70	1	121.338	133.011	125.624	98.605	119.644	219.982
13	80	70	1	72.046	110.188	86.920	83.434	88.147	256.256
14	70	70	1	90.655	64.849	61.258	94.445	77.802	294.561
15	60	70	1	43.885	33.856	43.773	50.523	43.009	47.194
...	...	...	...	...	...	...	...	...	...
76	50	100	1	30.462	24.011	23.949	24.101	25.631	10.378
77	40	100	1	17.728	27.146	20.837	20.911	21.655	15.598
78	30	100	1	17.787	23.930	24.039	24.053	22.452	9.676
79	20	100	1	20.837	14.670	11.634	17.710	16.213	15.656
80	10	100	1	14.644	14.708	5.722	11.666	11.685	17.816

 DOI: 10.25077/josi.v23.n1.p76-91.2024

Table 4. Analysis of Variance

Source	DF	Adj SS	Adj MS	F-Value	P-Value
Model	8	166015	20752	202.33	0.000
Linear	3	140038	46679	455.13	0.000
X1	1	130584	130584	1273.21	0.000
X2	1	4971	4971	48.47	0.000
X3	1	4483	4483	43.71	0.000
Square	2	25037	12519	122.06	0.000
X1*X1	1	25022	25022	243.97	0.000
X2*X2	1	15	15	0.15	0.701
2-Way Interaction	3	940	313	3.05	0.034
X1*X2	1	31	31	0.30	0.583
X1*X3	1	741	741	7.23	0.009
X2*X3	1	167	167	1.63	0.206
Error	71	7282	103		
Total	79	173297			

From these results, we can derive several insights. Firstly, the P-values indicate that these variables and their interactions have statistically significant effects on the dependent variable, suggesting that their effects are unlikely due to random variation. Specifically, X1, X2, and X3 each have significant individual impacts on the outcome variable. The significance of X1*X1 suggests a quadratic relationship, indicating that the effect of X1 on the dependent variable follows a parabolic pattern, implying diminishing returns or an optimal level. The significance of the interaction term X1*X3 suggests that the effect of X1 depends on the level of X3, indicating complex interdependencies. These results imply that the model fits the data well, capturing important relationships, and that the relationships between the predictors and the dependent variable are intricate, involving both linear and nonlinear effects. This complexity should be considered in decision-making and further analysis to optimize outcomes based on X1, X2, and X3. The significant effects of X1, X2, X3, X1*X1, and X1*X3 on Y are illustrated in Figure 8.

The regression model in Response Surface Methodology (RSM) is crucial for exploring and optimizing the relationships between multiple independent variables and one or more dependent variables [51]. Its primary goal is

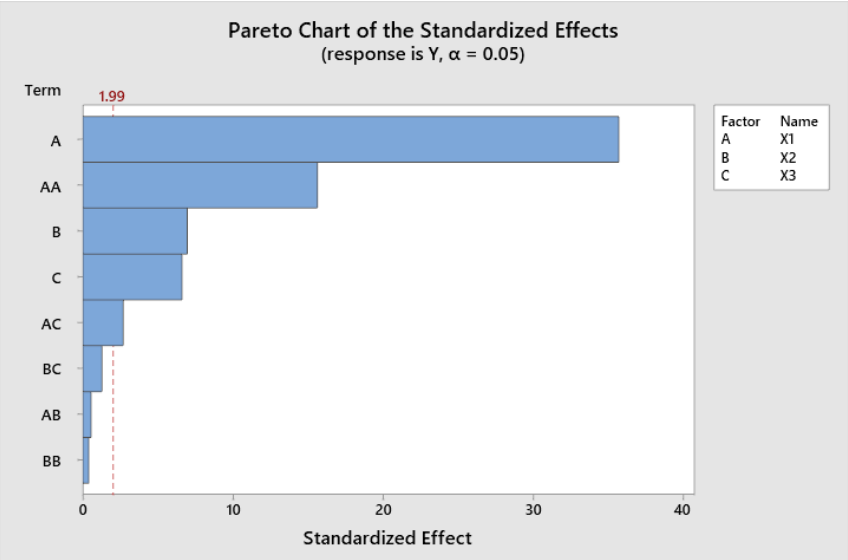

Figure 8. Pareto Chart of the Standardized Effects

Table 5. Goodness of statistics in Regression Model

S	R-sq (R^2)	R^2 (adj)	R^2 (pred)
10.1273	95.80%	95.32%	94.71%

to identify the optimal levels of the independent variables that either maximize or minimize the response, thus facilitating process optimization. The regression equations for the model are presented in Equation (11) for X3 = 0 and Equation (12) for X3 = 1.

$$Y = 135.6 - 0.999X1 - 1.47X2 + 0.02434X1^2 + 0.0044X2^2 - 0.00195X1X2 \quad (11)$$

$$Y = 110.3 - 1.211X1 - 1.21X2 + 0.02434X1^2 + 0.0044X2^2 - 0.00195X1X2 \quad (12)$$

R-square (R^2) plays a critical role in assessing the quality of a regression model. Table 5 presents the R^2 value, which quantifies the proportion of variance in the dependent variable explained by the independent variables in the model. The R^2 value of 95.80% suggests an excellent fit, indicating that the model accounts for a substantial portion of the variability in the response variable.

While the R^2 provides an overall measure of goodness of fit, it is essential to consider Adjusted R^2 and Predicted R^2 for a more nuanced evaluation. Adjusted R^2 adjusts for the number of predictors in the model, offering a more accurate metric when comparing models with different numbers of independent variables. This adjustment prevents overestimation of the goodness of fit by penalizing the inclusion of extraneous predictors. Predicted R^2, on the other hand, assesses the model's predictive capability, specifically its performance in predicting new observations. This measure accounts for both the number of predictors and the accuracy of the model in predicting new data points. A higher Predicted R^2 value signifies superior predictive performance, indicating that the model is more reliable when applied to unseen data [52], [53]. It is particularly useful in assessing the model's ability to make accurate predictions outside the range of the training data. In this case, a Predicted R^2 value of 94.71% indicates a good fit for predicting new data.

The analysis of the relationship between each independent variable (X1, X2, and X3) and the dependent variable (Y), as depicted in Figure 9, reveals nuanced dynamics. The data indicates a strong positive correlation between X1 and Y: as the value of X1 increases, the value of Y correspondingly rises, suggesting that improvements in X1 directly contribute to enhancements in Y. Conversely, X2 shows a significant negative correlation with Y. An increase in X2 leads to a decrease in Y, indicating that higher values of X2 may hinder or reduce the value of Y. For X3, the pattern of influence is more complex. The cubic infill pattern associated with X3 exerts a stronger effect on Y compared to the grid infill pattern. This suggests that the structure or method represented by the cubic infill is more effective or

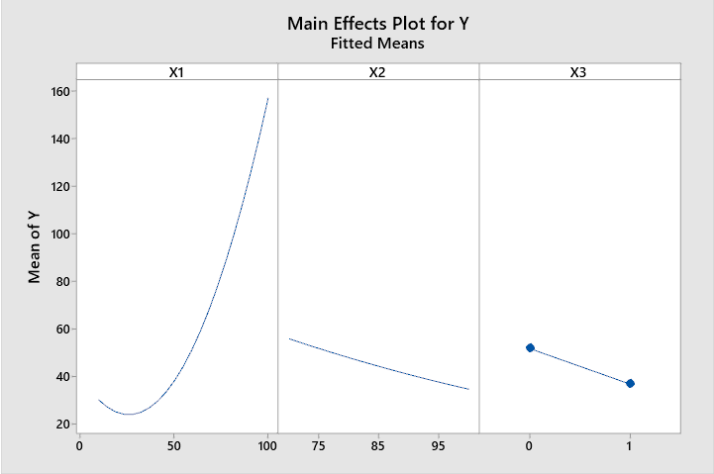

Figure 9. Individual relation of independent variable vs dependent variable

 DOI: 10.25077/josi.v23.n1.p76-91.2024

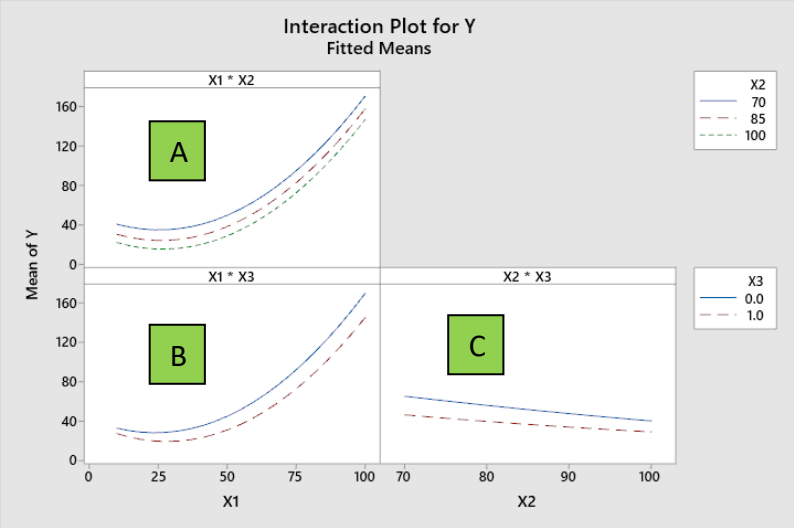

Figure 10. Interaction relation of independent variable vs dependent variable

has a greater impact on Y than the grid infill. These insights point to targeted areas for further investigation and optimization. Specifically, it is important to focus on the mechanisms through which X1 enhances Y, the factors driving the inverse relationship between X2 and Y, and the specific attributes of the cubic infill pattern that make it more influential on Y.

Unlike individual relationships, Figure 10 illustrates the interaction plot for the values of Y with combinations of X. Part A of Figure 10 shows a positive interaction between X1 and X2 on Y. The blue line, red dashed line, and green dashed line have similar shapes, but to achieve better strength with the same X1 value, it is advisable to use a smaller X2 value (X2 = 70; blue line). In part B of Figure 10, the interaction between X1 and X3 on Y is depicted. The blue line represents the scenario when X3 is cubic, while the red dashed line represents the scenario when X3 is grid. This indicates that using a cubic infill pattern (X3 = 0) with the same X1 value generally produces better Y values. Part C of Figure 10 illustrates the relationship between X2 and X3 on Y, showing that using the same X2 value will yield a better Y value if X3 is cubic (X3 = 0). These interaction plots reveal that the combination of a lower X2 value and a cubic infill pattern generally enhances the strength (Y), highlighting the importance of considering these interactions in optimizing 3D printing parameters.

Figure 11 (left side) shows the relationship between X1, X2, and Y with X3 = 0. The dark blue area represents low Y values, while the dark green area indicates high Y values. When X1 exceeds 50%, the influence of X2 becomes

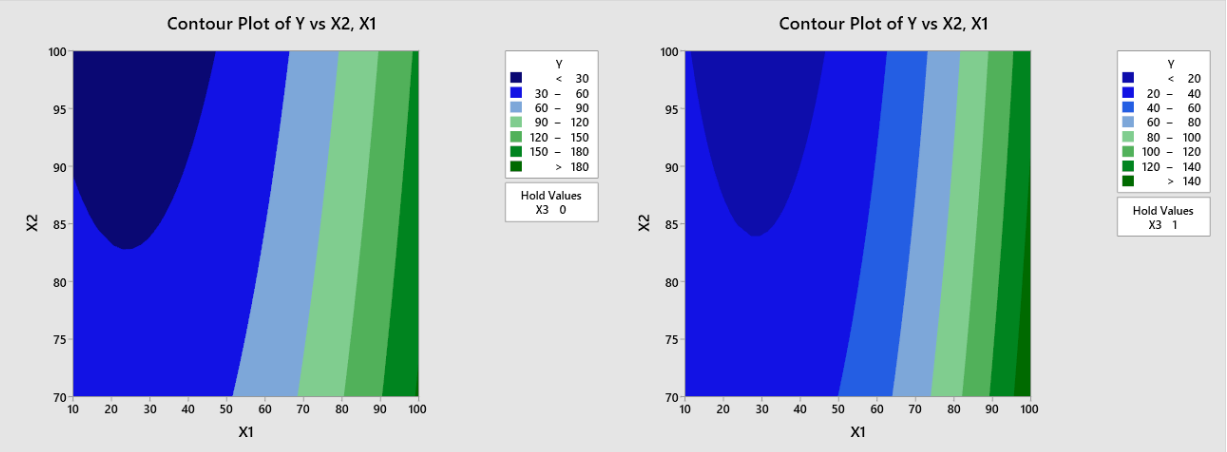

Figure 11. Contour Plot X1, X2, X3 = 0 vs Y and Contour Plot X1, X2, X3 = 1 vs Y

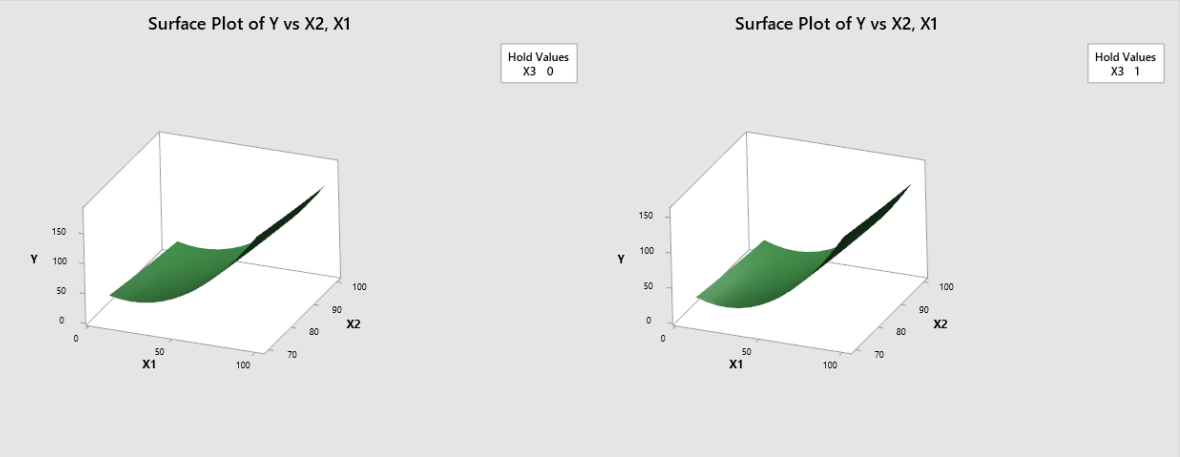

Figure 12. Surface Plot X1, X2, X3 = 0 vs Y and Surface Plot X1, X2, X3 =1 vs Y

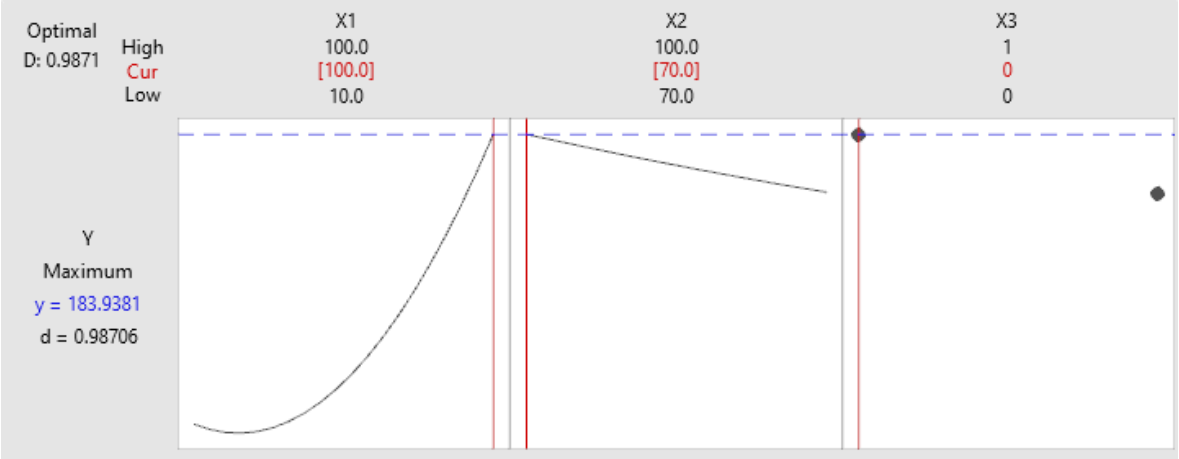

Figure 13. Chart of maximum solution of Y

insignificant. Thus, for high-speed printing, an infill density greater than 50% is advisable. However, if the infill density is less than 50%, the recommended printing speed is under 80mm/s. Figure 11 (right side) depicts the relationship between X1, X2, and Y with X3 = 1. Again, the dark blue area indicates low Y values, and the dark green area indicates high Y values. Here, Y values tend to stabilize for various X2 values when X1 is greater than 60%. However, if X1 is less than 60%, the recommended X2 value is under 80mm/s. It is clear from Figure 11 that the Y value cannot reach its maximum if the printing speed exceeds 90mm/s, even with a 100% infill density.

While Figure 11 provides a 2D contour plot, Figure 12 offers a 3D surface plot. Figure 12 (left side) is a surface plot for X3 = 0, and Figure 12 (right side) is a surface plot for X3 = 1. These surface plots help identify the global maximum value for Y. Table 6 and Figure 13 demonstrate that the optimal values for X1, X2, and X3 result in the highest Y value. This result reveals that the best combination of parameters for attaining the highest impact strength (Y) involves setting the infill density (X1) to 100%, using a printing speed (X2) of 70mm/s, and employing a cubic infill pattern (X3). This specific combination yields an optimal Y value of 183.938 kJ/m². The reliability of these findings is underscored by the 95% confidence interval for the maximum Y value, which ranges from 174.19 to 193.69 kJ/m², and the 95% prediction interval, which spans from 161.51 to 206.36 kJ/m².

Table 6. Maximum solution of Y

X1	X2	X3	Y fit	SE fit	95% CI	95% PI
100	70	0	183.938	4.89	(174.19, 193.69)	(161.51, 206.36)

 DOI: 10.25077/josi.v23.n1.p76-91.2024

Further insights into the influence of individual parameters show that increasing the infill density to 100% significantly enhances the strength of the printed object. The study also highlights that a moderate printing speed of 70mm/s is optimal, as higher speeds may compromise the material's strength. Additionally, the cubic infill pattern proves to be more effective than the grid pattern in achieving superior strength. The 3D surface plots used in the analysis illustrate the interactions between these parameters, consistently showing that a high infill density combined with a cubic pattern yields the best results.

CONCLUSION

To conclude, our study integrates these three critical parameters to determine their optimal values for 3D printing. Our primary recommendations for achieving optimal strength include setting the infill density to 100%, using a printing speed of 70mm/s, and employing the cubic infill pattern. However, further analysis reveals nuances that can guide practical implementation. For instance, we found that an infill density exceeding 50%, combined with the cubic infill pattern, allows users to increase the printing speed to 100mm/s without a significant reduction in strength. Conversely, for lightweight printing, we recommend using infill densities below 50%, paired with the cubic infill pattern and printing speeds under 80mm/s. It is important to note that our study is just a stepping stone in understanding the complex interplay of printing parameters. Future research could explore additional factors, such as enclosure printing techniques or post-printing annealing processes, to further enhance product strength and expand the applicability of 3D printing in various industries. By providing these insights, we contribute not only to the technical understanding within the research domain but also offer practical guidelines for practitioners seeking to optimize their 3D printing processes for diverse applications.

ACKNOWLEDGMENT

We sincerely thank the editor and the anonymous reviewers for their invaluable time, expertise, and constructive feedback. Their thoughtful comments and insightful suggestions significantly enhanced and refined this manuscript. We greatly appreciate their dedication to maintaining the quality and rigor of the academic publication process.

CONFLICT OF INTEREST

The authors declare no conflicts of interest that could potentially compromise the objectivity, impartiality, or credibility of the research presented in this article.

FUNDING

The authors did not receive any financial support for the research, writing, or publication of this article.

References

[1] J. Teixeira, C. O. Schaefer, B. Rangel, L. Maia, and J. L. Alves, “A road map to find in 3D printing a new design plasticity for construction – The state of art,” Frontiers of Architectural Research, vol. 12, no. 2. 2023. doi: 10.1016/j.foar.2022.10.001.

[2] O. Abdulhameed, A. Al-Ahmari, W. Ameen, and S. H. Mian, “Additive manufacturing: Challenges, trends, and applications,” Advances in Mechanical Engineering, vol. 11, no. 2, 2019, doi: 10.1177/1687814018822880.

[3] J. Zhu, H. Zhou, C. Wang, L. Zhou, S. Yuan, and W. Zhang, “A review of topology optimization for additive manufacturing: Status and challenges,” Chinese Journal of Aeronautics, vol. 34, no. 1. 2021. doi: 10.1016/j.cja.2020.09.020.

[4] Mikell P. Groover, Fundamentals of Modern Manufacturing Materials, Processes, and Systems Seventh Edition, vol. 53, no. 9. 2020.

[5] J. Y. Lee, J. An, and C. K. Chua, “Fundamentals and applications of 3D printing for novel materials,” Applied Materials Today, vol. 7. 2017. doi: 10.1016/j.apmt.2017.02.004.

[6] S. Rouf et al., "Additive manufacturing technologies: Industrial and medical applications," Sustainable Operations and Computers, vol. 3, 2022, doi: 10.1016/j.susoc.2022.05.001.
[7] M. Salmi, "Additive manufacturing processes in medical applications," Materials, vol. 14, no. 1. 2021. doi: https://doi.org/10.3390/ma14010191.
[8] B. Blakey-Milner et al., "Metal additive manufacturing in aerospace: A review," Mater Des, vol. 209, 2021, doi: 10.1016/j.matdes.2021.110008.
[9] G. Liu et al., "Additive manufacturing of structural materials," Materials Science and Engineering R: Reports, vol. 145. 2021. doi: 10.1016/j.mser.2020.100596.
[10] U. M. Dilberoglu, B. Gharehpapagh, U. Yaman, and M. Dolen, "The Role of Additive Manufacturing in the Era of Industry 4.0," Procedia Manuf, vol. 11, 2017, doi: 10.1016/j.promfg.2017.07.148.
[11] M. K. Thompson et al., "Design for Additive Manufacturing: Trends, opportunities, considerations, and constraints," CIRP Ann Manuf Technol, vol. 65, no. 2, 2016, doi: 10.1016/j.cirp.2016.05.004.
[12] A. Townsend, N. Senin, L. Blunt, R. K. Leach, and J. S. Taylor, "Surface texture metrology for metal additive manufacturing: a review," Precision Engineering, vol. 46. 2016. doi: 10.1016/j.precisioneng.2016.06.001.
[13] A. Majeed et al., "A big data-driven framework for sustainable and smart additive manufacturing," Robot Comput Integr Manuf, vol. 67, 2021, doi: 10.1016/j.rcim.2020.102026.
[14] M. Javaid, A. Haleem, R. P. Singh, R. Suman, and S. Rab, "Role of additive manufacturing applications towards environmental sustainability," Advanced Industrial and Engineering Polymer Research, vol. 4, no. 4. 2021. doi: 10.1016/j.aiepr.2021.07.005.
[15] J. Jiang, X. Xu, and J. Stringer, "Support structures for additive manufacturing: A review," Journal of Manufacturing and Materials Processing, vol. 2, no. 4. 2018. doi: https://doi.org/10.3390/jmmp2040064.
[16] Y. Zhang et al., "Additive Manufacturing of Metallic Materials: A Review," Journal of Materials Engineering and Performance, vol. 27, no. 1. 2018. doi: 10.1007/s11665-017-2747-y.
[17] S. Ford and M. Despeisse, "Additive manufacturing and sustainability: an exploratory study of the advantages and challenges," J Clean Prod, vol. 137, 2016, doi: 10.1016/j.jclepro.2016.04.150.
[18] N. Krajangsawasdi, L. G. Blok, I. Hamerton, M. L. Longana, B. K. S. Woods, and D. S. Ivanov, "Fused deposition modelling of fibre reinforced polymer composites: A parametric review," Journal of Composites Science, vol. 5, no. 1. 2021. doi: 10.3390/jcs5010029.
[19] R. B. Kristiawan, F. Imaduddin, D. Ariawan, Ubaidillah, and Z. Arifin, "A review on the fused deposition modeling (FDM) 3D printing: Filament processing, materials, and printing parameters," Open Engineering, vol. 11, no. 1. 2021. doi: 10.1515/eng-2021-0063.
[20] S. Wickramasinghe, T. Do, and P. Tran, "FDM-Based 3D printing of polymer and associated composite: A review on mechanical properties, defects and treatments," Polymers, vol. 12, no. 7. 2020. doi: 10.3390/polym12071529.
[21] S. Wasti and S. Adhikari, "Use of Biomaterials for 3D Printing by Fused Deposition Modeling Technique: A Review," Frontiers in Chemistry, vol. 8. 2020. doi: 10.3389/fchem.2020.00315.
[22] A. D. Valino, J. R. C. Dizon, A. H. Espera, Q. Chen, J. Messman, and R. C. Advincula, "Advances in 3D printing of thermoplastic polymer composites and nanocomposites," Progress in Polymer Science, vol. 98. 2019. doi: 10.1016/j.progpolymsci.2019.101162.
[23] H. Bakhtiari, M. Aamir, and M. Tolouei-Rad, "Effect of 3D Printing Parameters on the Fatigue Properties of Parts Manufactured by Fused Filament Fabrication: A Review," Applied Sciences (Switzerland), vol. 13, no. 2. 2023. doi: 10.3390/app13020904.
[24] N. Maqsood and M. Rimašauskas, "Delamination observation occurred during the flexural bending in additively manufactured PLA-short carbon fiber filament reinforced with continuous carbon fiber composite," Results in Engineering, vol. 11, 2021, doi: 10.1016/j.rineng.2021.100246.
[25] S. Hwang, E. I. Reyes, K. sik Moon, R. C. Rumpf, and N. S. Kim, "Thermo-mechanical Characterization of Metal/Polymer Composite Filaments and Printing Parameter Study for Fused Deposition Modeling in the 3D Printing Process," J Electron Mater, vol. 44, no. 3, 2015, doi: 10.1007/s11664-014-3425-6.
[26] M. León-Calero, S. C. Reyburn Valés, Á. Marcos-Fernández, and J. Rodríguez-Hernandez, "3D printing of thermoplastic elastomers: Role of the chemical composition and printing parameters in the production of parts

with controlled energy absorption and damping capacity," Polymers (Basel), vol. 13, no. 20, 2021, doi: 10.3390/polym13203551.

[27] C. R. Tripathy, R. K. Sharma, and V. K. Rattan, "Effect of printing parameters on the mechanical behaviour of the thermoplastic polymer processed by FDM technique: A research review," Advances in Production Engineering And Management, vol. 17, no. 3, 2022, doi: 10.14743/apem2022.3.436.

[28] R. A. Ilyas et al., "Natural Fiber-Reinforced Polylactic Acid, Polylactic Acid Blends and Their Composites for Advanced Applications," Polymers, vol. 14, no. 1. 2022. doi: 10.3390/polym14010202.

[29] L. Ranakoti et al., "Critical Review on Polylactic Acid: Properties, Structure, Processing, Biocomposites, and Nanocomposites," Materials, vol. 15, no. 12. 2022. doi: 10.3390/ma15124312.

[30] S. Pérez-Davila et al., "3D-Printed PLA Medical Devices: Physicochemical Changes and Biological Response after Sterilisation Treatments," Polymers (Basel), vol. 14, no. 19, 2022, doi: 10.3390/polym14194117.

[31] J. S. Bergström and D. Hayman, "An Overview of Mechanical Properties and Material Modeling of Polylactide (PLA) for Medical Applications," Ann Biomed Eng, vol. 44, no. 2, 2016, doi: 10.1007/s10439-015-1455-8.

[32] T. Grethe, "Biodegradable synthetic polymers in textiles – what lies beyond pla and medical applications? A review.," Tekstilec, vol. 64, no. 1, 2021, doi: https://doi.org/10.14502/Tekstilec2021.64.32-46.

[33] N. A. A. B. Taib et al., "A review on poly lactic acid (PLA) as a biodegradable polymer," Polymer Bulletin, vol. 80, no. 2. 2023. doi: 10.1007/s00289-022-04160-y.

[34] E. H. Tümer and H. Y. Erbil, "Extrusion-based 3d printing applications of pla composites: A review," Coatings, vol. 11, no. 4. 2021. doi: 10.3390/coatings11040390.

[35] Z. Kovačević, S. Bischof, E. Vujasinović, and M. Fan, "The potential of nanoclay modified Spartium junceum L. Fibres used as reinforcement in PLA matrix composites for automotive applications," Int J Nanotechnol, vol. 15, no. 8–10, 2018, doi: 10.1504/IJNT.2018.098436.

[36] C. Ciofu, S. N. Mazurchevici, D. Maldonado-Cortes, L. Pena-Paras, D. I. Q. Correa, and D. Nedelcu, "Tribological behavior of PLA biodegradable materials used in the automotive industry," International Journal of Modern Manufacturing Technologies, vol. 11, no. 3 Special Issue, 2019.

[37] Z. Liu, Y. Wang, B. Wu, C. Cui, Y. Guo, and C. Yan, "A critical review of fused deposition modeling 3D printing technology in manufacturing polylactic acid parts," International Journal of Advanced Manufacturing Technology, vol. 102, no. 9–12. 2019. doi: 10.1007/s00170-019-03332-x.

[38] M. H. Hsueh et al., "Effect of printing parameters on the thermal and mechanical properties of 3d-printed pla and petg, using fused deposition modeling," Polymers (Basel), vol. 13, no. 11, 2021, doi: 10.3390/polym13111758.

[39] P. Yadav, A. Sahai, and R. S. Sharma, "Experimental Studies on the Mechanical Behaviour of Three-Dimensional PLA Printed Parts by Fused Filament Fabrication," Journal of The Institution of Engineers (India): Series D, vol. 104, no. 1, 2023, doi: 10.1007/s40033-022-00403-4.

[40] F. Yilan, İ. B. Şahin, F. Koç, and L. Urtekin, "The Effects of Different Process Parameters of PLA+ on Tensile Strengths in 3D Printer Produced by Fused Deposition Modeling," El-Cezeri Journal of Science and Engineering, vol. 10, no. 1, 2023, doi: 10.31202/ecjse.1179492.

[41] A. D. Tura, H. G. Lemu, L. E. Melaku, and H. B. Mamo, "Impact of FDM 3D Printing Parameters on Compressive Strength and Printing Weight of PLA Components," in Lecture Notes in Electrical Engineering, 2023. doi: 10.1007/978-981-19-9338-1_60.

[42] V. V. Bhandarkar, I. G. Patil, H. Y. Shahare, and P. Tandon, "Understanding The Influence of Process Parameters oor Minimizing Defects on 3d Printed Parts through Remote Monitoring," in ASME International Mechanical Engineering Congress and Exposition, Proceedings (IMECE), 2022. doi: 10.1115/IMECE2022-93991.

[43] M. Mani, A. G. Karthikeyan, K. Kalaiselvan, P. Muthusamy, and P. Muruganandhan, "Optimization of FDM 3-D printer process parameters for surface roughness and mechanical properties using PLA material," Mater Today Proc, vol. 66, 2022, doi: 10.1016/j.matpr.2022.05.422.

[44] A. Mishra, V. Srivastava, and N. K. Gupta, "Additive manufacturing for fused deposition modeling of carbon fiber–polylactic acid composites: the effects of process parameters on tensile and flexural properties," Functional Composites and Structures, vol. 3, no. 4, 2021, doi: 10.1088/2631-6331/ac3732.

[45] J. A. Travieso-Rodriguez, R. Jerez-Mesa, J. Llumà, G. Gomez-Gras, and O. Casadesus, "Comparative study of the flexural properties of ABS, PLA and a PLA–wood composite manufactured through fused filament fabrication," Rapid Prototyp J, vol. 27, no. 1, 2021, doi: 10.1108/RPJ-01-2020-0022.

[46] G. N. Khawly, N. R. Fabbri, A. J. W. McClung, and J. D. Ocampo, "Impact Testing of a Commercial Poly-Lactic Acid," in Conference Proceedings of the Society for Experimental Mechanics Series, 2021. doi: 10.1007/978-3-030-59765-8_2.

[47] A. Pandzic, D. Hodzic, I. Hajro, and P. Tasic, "Strength properties of PLA material obtained by different models of FDM 3D printer," in Annals of DAAAM and Proceedings of the International DAAAM Symposium, 2020. doi: 10.2507/31st.daaam.proceedings.044.

[48] M.S. Hasan, T. Ivanov, M. Vorkapic, A. Simonovic, D. Daou, A. Kovacevic, A. Milovanovic, "Impact of aging effect and heat treatment on the tensile properties of PLA (poly lactic acid) printed parts," Materiale Plastice, vol. 57, no. 3, 2020, doi: 10.37358/MP.20.3.5389.

[49] J. Triyono, H. Sukanto, R. M. Saputra, and D. F. Smaradhana, "The effect of nozzle hole diameter of 3D printing on porosity and tensile strength parts using polylactic acid material," Open Engineering, vol. 10, no. 1, 2020, doi: 10.1515/eng-2020-0083.

[50] P. K. Farayibi and B. O. Omiyale, "Mechanical behaviour of polylactic acid parts fabricated via material extrusion process: A taguchi-grey relational analysis approach," International Journal of Engineering Research in Africa, vol. 46, 2020, doi: 10.4028/www.scientific.net/JERA.46.32.

[51] F. Wajdia and M. S. Saad, "Optimizing Surface Finish and Dimensional Accuracy in 3D Printed Free-Form Objects," Jurnal Optimasi Sistem Industri, vol. 22 no. 2 (2023), doi: 10.25077/josi.v22.n2.p99-113.2023.

[52] S. M. Ross, Introduction to Probability and Statistics for Engineers and Scientists, Sixth Edition. 2020. doi: 10.1016/C2018-0-02166-0.

[53] R. H. Myers and S. L. Myers, Probability & Statistics for Engineers Scientists Probability & Statistics for Engineers & Scientists, vol. 6. 2007.

AUTHORS BIOGRAPHY

Engelbert Harsandi Erik Suryadarma is a doctoral student in the Department of Industrial Engineering at Universitas Sebelas Maret Surakarta. He holds a Bachelor of Engineering (S.T.) and a Master of Engineering (M.T.) from the Department of Industrial Engineering at Universitas Atma Jaya Yogyakarta, and an Engineering degree (Ir.) from Universitas Gadjah Mada Yogyakarta. His research interests encompass a wide range of topics, including industrial automation, robotics, artificial intelligence, design engineering, and manufacturing engineering.

Pringgo Widyo Laksono is a senior lecturer in Industrial Engineering and a researcher in the Production System Laboratory at Universitas Sebelas Maret, Surakarta, Indonesia. His research interests include automation and production systems, human-machine interaction, intelligent machines, ergonomics, and production development systems engineering. He is also interested in optimization, modeling, AI, mechatronics, and CAE. Currently, he is pursuing PhD research on controlling robotic arms based on biosignals at Gifu University, Japan.

Ilham Priadythama is a senior lecturer in Industrial Engineering at Universitas Sebelas Maret, Surakarta, Indonesia. He earned his Doctor of Engineering (Dr. Eng.) from Gifu University, Japan. His research interests focus on biomechanics, assistive technology, and product development.